Journal of Alloys and Compounds 1014 (2025) 178693

Contents lists available at ScienceDirect

Journal of Alloys and Compounds

journal homepage: www.elsevier.com/locate/jalcom

Influence of hydrogen on the γ-matrix lattice parameters of a Ni-based superalloy – A synchrotron diffraction study

Massimo Fritton [a,*], Alexander Mutschke [a], Oliver Nagel [b], Andreas Stark [c], Masood Hafez-Haghighat [d], Bodo Gehrmann [d], Steffen Neumeier [b], Ralph Gilles [a]

[a] Technische Universität München, Lichtenbergstr. 1, Garching 85748, Germany
[b] Friedrich-Alexander-Universität Erlangen-Nürnberg, Martensstr. 5, Erlangen 91058, Germany
[c] Helmholtz-Zentrum hereon GmbH, Max-Planck-Straße 1, Geesthacht 21502, Germany
[d] VDM Metals International GmbH, Zeilweg 42, Frankfurt am Main 65439, Germany

ARTICLE INFO

Keywords:
Ni-based superalloys
Hydrogen embrittlement (HE)
High-energy X-ray diffraction (HEXRD)
Lattice parameter expansion
Fracture surface
Hydrogen effusion
Tensile tests

ABSTRACT

Hydrogen, as an energy carrier, is expected to play a significant role in future mobility. The objective of this study was to investigate the hydrogen uptake of the Ni-based superalloy VDM® Alloy 780 through electrochemical charging, using high-energy synchrotron X-ray diffraction (HEXRD). It is shown that the incorporation of hydrogen at interstitial positions in the crystal lattice leads to a slight increase in the lattice parameters compared to hydrogen-free analogs. In-situ HEXRD measurements showed a convergence of the lattice parameters at elevated temperatures, indicating the reversibility of hydrogenation through diffusion and subsequent effusion of hydrogen. Hot gas extraction (HGE) measurements were conducted to quantify hydrogen and complement the diffraction data, showing that prolonged electrochemical charging leads to increased hydrogen content. Hydrogen quantification at different temperatures confirmed increasing diffusion with temperature, i.e. higher measured hydrogen values at elevated temperatures. Additionally, tensile tests were conducted to evaluate the influence of hydrogen on the alloy during deformation. Fractographic analysis via SEM showed that, for the hydrogen-treated specimen, cleavage fracture occurred in the vicinity of the surface, whereas the reference sample displayed typical ductile fracture patterns over the entire fracture surface.

1. Introduction

To move away from the dependency on fossil fuels and achieve carbon neutrality, hydrogen has been singled out as a key technology. Hydrogen-based energy infrastructure may help in evolving our energy systems by providing an unlimited reservoir and enabling emission-free combustion to reduce CO_2 pollution. Hydrogen can serve as an energy carrier or as a feedstock. Furthermore, hydrogen can be used to store seasonal fluctuating amounts of renewable electricity. The use of hydrogen as a fuel in jet engines or gas turbines is, however, an ambitious goal. One particular problem could be the failure of components due to hydrogen embrittlement (HE), which has been observed in various industrial systems, including high-pressure hydrogen storage tanks or pipelines. This could occur in aircraft components as well, which are made of high-strength nickel-based superalloys or stainless steel [1–3]. HE of alloys and its underlying mechanisms remains a major challenge for material science and will become even more important with the surging use of hydrogen as an energy carrier. Materials subjected to high tensile loads under the influence of hydrogen can change their deformation characteristics, i.e. a transition from ductile to brittle with a decreased elongation at fracture [4,5]. Many hypotheses concerning the cause of HE were addressed in the past. Yet, a conclusive, encompassing explanation is still lacking. The two most prominent mechanisms explaining hydrogen embrittlement are: a) Hydrogen Induced Decohesion (HEDE) where absorbed hydrogen atoms lower the cohesive strength by dilatation of the atomic lattice leading to reduced material ductility and increased susceptibility to cracking [6–8]. b) Hydrogen Enhanced Localized Plasticity (HELP) is another mechanism, wherein hydrogen atoms promote localized plastic deformation, causing strain concentration and crack initiation, ultimately compromising the material's mechanical properties and fracture toughness [9,10].

One of the main reasons for the unclear and often contradictory description of HE is the difficulty of directly detecting and analysing the light chemical element hydrogen in materials. Hydrogen is basically

* Corresponding author.
E-mail address: Massimo.Fritton@frm2.tum.de (M. Fritton).

https://doi.org/10.1016/j.jallcom.2025.178693
Received 8 October 2024; Received in revised form 13 January 2025; Accepted 14 January 2025
Available online 15 January 2025

invisible to X-rays due to its low electron density and accordingly its low scattering power. Therefore, a large number of analytical methods are inapplicable. Additionally, only small amounts of hydrogen are introduced into alloys, i.e. 0–100 wt. ppm, impeding its detection possibilities even further. In summary, localization and quantification of hydrogen introduced into the material is in general a challenging task. Prompt Gamma Activation Analysis (PGAA) offers a non-destructive technique for the quantification of hydrogen [11], however, the high Co amount in the VDM® Alloy 780, which is investigated in this study, impedes its application as the hydrogen and Co spectral lines are overlapping. As an alternative, the hydrogen content can be quantified via thermal methods, whereby the hydrogen is extracted from a sample with the aid of heat. The effusing hydrogen is then detected. For instance, Thermal Desorption Spectroscopy (TDS) is a technique where a specimen is heated under ultra-high vacuum conditions and the released hydrogen is ionized and detected by a mass spectrometer [12]. A benefit of this technique is the possibility of correlating the effusion temperatures of the hydrogen to specific positions in the microstructure [13]. Another thermal technique is Hot Gas Extraction (HGE) which is based on a thermal conductivity change of a carrier gas by the release of molecular hydrogen by heating or melting the sample [14]. A major drawback of such thermal methods is the inevitable destruction or modification of the samples by the heat treatment and that solely effusing hydrogen is measured, i.e. molecular hydrogen is measured outside the material.

To understand HE, processes at the atomic level arising due to the incorporation of hydrogen must be investigated. In this case, diffraction techniques are the method of choice for polycrystalline alloys, as they allow the identification and quantification of different phases, and precise determination of lattice parameters. While X-ray and neutron diffraction are mainly used for structure elucidation, a variety of material properties can be investigated based on these analytical methods. For instance, absorbed hydrogen leads to internal strain, i.e. slight changes in the interatomic distances that can be detected by diffraction techniques [15,16]. However, the consideration of lattice parameters as a result of hydrogen absorption has only been studied sparsely so far. In this study, we want to highlight the power of using diffraction as a non-destructive tool for the quantification of hydrogen effects. For this purpose, a comparatively simple, i.e. completely austenitic system is investigated, which can be obtained from the Ni-base superalloy VDM® Alloy 780 by solution annealing and water quenching to first dissolve and then suppress the precipitation of hardening and high temperature phases. VDM® Alloy 780 has been developed to enhance mechanical properties at elevated temperatures, thereby enabling its utilization in environments with working temperatures of up to 750 °C. In the fully hardened state, this superalloy exhibits a microstructure composed of an austenitic matrix (γ phase) strengthened by nano-sized intermetallic precipitates of Ni_3Al (γ'-phase) and high-temperature stable phases, i.e. Ni_3Nb-based (δ) and Ni_3Ti-based (η) phases [17–20]. The differences in the chemical composition and the microstructure of the VDM® Alloy 780 to the widely applied Alloy 718 were already discussed, with the important difference that no γ′ is formed in VDM® Alloy 780 [20–25]. From tensile tests it is known that γ′ increases the susceptibility to HE for Alloy 718, leading to reduced elongation at fracture values [26,27]. One reason for this is that the coherent phase boundary between γ and γ′ is a preferred hydrogen adsorption site [28]. Under load, the aforementioned HEDE, HELP, or a combination of both mechanisms can lead to premature failure under load [3]. Since precipitation of γ′ is hindered in VDM® Alloy 780 which is known to enhance HE, the alloy is a potential candidate for applications in hydrogen-containing environments. In addition, the δ phase also has an effect on the sensitivity to HE in Alloy 718. The higher the content, the stronger the embrittlement, i.e. the lower the tensile strength [27,29]. Therefore, it is also noteworthy that VDM® Alloy 780 has a lower fraction of such high-temperature precipitate phases compared to Alloy 718 [30].

Most of the existing publications quantify HE in polycrystalline superalloys by either pre-charging specimens before tensile testing with hydrogen or by in-situ charging during tensile deformation [27,29,31–34]. The elongation at fracture value is used as a measure for HE with decreasing values indicating brittle fracture due to the loss of ductility. Additionally, the fracture surfaces can be evaluated after the experiment. Ni-base superalloys are generally characterized by a ductile behavior and a fracture surface of primarily micro-void coalescence in the absence of hydrogen [35,36]. Increasing the amount of hydrogen in the material leads to a decreasing ductility and a more brittle fracture. The fracture surface of hydrogen-loaded specimens is characterized by transgranular cracking and intergranular cracking. This study shows an alternative approach to understanding the effects of hydrogen absorbed in alloys. The incorporation of hydrogen at interstitial sites, specifically octahedral or tetrahedral sites within the fcc lattice, results in an expansion of the host lattice due to the space required for the absorbed hydrogen [37]. Synchrotron diffraction is used to test whether the absorbed hydrogen causes measurable changes in the interatomic distances. Therefore, the lattice parameters are always measured in relation to an unloaded reference sample, which is identical except for the added hydrogen. XRD provides an indirect proof of the presence of hydrogen, as the only observable consequence of its presence is a change in the spacing of metal atoms. Comparatively, HGE is performed for the quantification of hydrogen contents. For this study, only fully solution annealed VDM® Alloy 780 is used comprising solely the austenitic γ-matrix, to perform the experiments with a comparatively simple model system.

2. Experimental

The starting material with the chemical composition shown in Table 1 for all the experiments in this study was solution annealed (1 h @ 1080 °C) and water-quenched VDM® Alloy 780 rod material from the same batch.

This heat treatment is abbreviated to WB0 in the following. All experiments were performed with cylindrical specimens with a diameter of 5 mm to ensure comparability. Electrochemical charging was performed for 24 h, 48 h, and 72 h with a current density of 40 mA/cm^2 at room temperature, controlled with a Gamry Interface 1010™ Galvanostat. The used electrolyte was a solution of demineralized water with 3 wt% sodium chloride (NaCl) and 3 g/L ammonium thiocyanate (NH_4SCN) as a recombination inhibitor.

High-energy X-ray diffraction (HEXRD) patterns in Debye–Scherrer geometry were recorded at the HEMS [39] beamline at PETRA III, DESY (Hamburg, Germany) using X-rays with a photon energy of 100 keV, corresponding to a wavelength of 0.124 Å. The X-ray beam was set to a cross-section of 1 mm^2. The patterns were recorded on a flat panel detector (XRD1621, Perkin Elmer, Norwalk, CT, USA) with a pixel size of (200) × (200) µm, a resolution of 2048 × 2048 pixels, and acquisition times of 2 s. Sample-to-detector distance was set to 1630 mm and complete Debye-Scherrer rings were recorded. Isotropic scattered photon data were reduced and integrated using the Fit2D program package [40]. Crystal structure refinement of X-ray diffraction data for the exact determination of lattice parameters and microstrains were conducted by the Rietveld method using the Fullprof program package [41]. The profile function of the reflections were fitted by the Thompson Cox Hastings approximations. For the refinement of the HEXRD data, Caglioti parameters (U, V, W) were determined beforehand by a full refinement of an externally measured LaB_6 powder standard sample. The sample displacement, cell parameters, strain, size, and isotropic

Table 1
Chemical composition of the main alloying elements VDM® Alloy 780 determined by EDX measurements [38].

	Ni	Co	Cr	Fe	Mo	Nb	Al	Ti
wt%	45.5	25.5	18	0.6	2.8	5.1	2	0.4

thermal displacement parameters were refined. Preferred orientation was fitted by the March-Dollase multi-axial model [42]. The background was corrected by linear interpolation of background points or the Chebyshev polynomial function for sequential refinement.

The amount of incorporated hydrogen in the alloys was determined via hot-gas extraction, using an H-500 Hydrogen Determinator (Eltra GmbH, Haan, Germany). Therefore, the respective samples were weighed and placed inside a tube furnace. The horizontally arranged glass tube is brought to the respective temperature on its side located in the furnace and when tilted, the sample slides into the measuring zone. The advantage of this technique is that the sample does not pass through the temperature ramp of the furnace, and is measured directly at the set temperature. For the measurements, a cylindrical sample was electrochemically loaded and cut into slices for hydrogen determination. The samples were measured until the hydrogen signal fell below a threshold value and the area under the signal curve was automatically integrated and converted into a hydrogen content in wt ppm. For the determination of the integral hydrogen content, samples were measured at 1000 °C to ensure a complete degassing of the sample. To determine diffusive hydrogen, the furnace temperature was set to respective values between 100 °C and 1000 °C. The measuring principle is based on a change in the thermal conductivity of a carrier gas due to the hydrogen released from the sample.

Microstructural analysis was performed using Zeiss XB 540 Dual-beam scanning electron microscopes (SEM). Images of the initial microstructure were taken in backscatter electron diffraction (BSD) contrast and for all images, an acceleration voltage of 20 kV was used.

Tensile tests were performed with an electromechanical testing machine (Instron, Norwood, Massachusetts) and a deformation rate of 1×10^{-4} s^{-1} until failure of the specimens. The miniaturized round bar specimens were manufactured by wire erosion with a diameter of 2.5 mm and a measuring length of 12.5 mm. A laser extensometer (Fiedler Optoelektronik GmbH, Lützen, Germany) was used to measure the deformation.

3. Results and discussion

The microstructure of the VDM® Alloy 780 after heat treatment, i.e. solution annealing at 1080 °C for one hour and then water quenching, is shown in Fig. 1a). The microstructure comprises γ grains ranging from 50 to 200 μm, excluding crystallographic twins, with no observable texture. No HT phases, which are usually observed at the γ grain boundaries, and no γ' precipitates can be found as shown in the SEM image with higher magnification (cf. Fig. 1b). The absence of the γ' precipitates in the VDM® Alloy 780 WB0 condition has already been proven with atom probe tomography measurements performed by Solis et al. [43] and XRD measurements [38]. The small white particles appearing in the microstructure are primary carbides formed during the solidification process of the alloy [20].

No differences in the SEM images of the hydrogenated vs. the reference specimen could be observed, therefore only two representative microscopy images of hydrogen-loaded specimens are shown. This leads to the conclusion, that hydrogen loading does not visibly alter the microstructure of the alloy.

To observe the influence of hydrogen on a finer length scale, high-energy synchrotron XRD was applied to investigate even marginal changes in the lattice parameter. Diffraction patterns were acquired after electrochemically loading specimens for 24, 48, and 72 h and referenced to a hydrogen-free analog.

In Fig. 2a) the experimental setup for the HEXRD experiments is shown schematically. The diffraction experiments were performed in Debye-Scherrer geometry with sample rotation to maximize grain statistics, i.e. the illuminated sample volume. This is particularly important because, as shown in Fig. 1, the γ grains are comparatively large. Since the diffraction patterns in Fig. 2b) (small inset) look almost identical, exclusively the 2θ range of the γ(311) Bragg reflection is depicted for improved visualization, showing decreasing 2θ values for the hydrogen-treated specimens. The Rietveld refinement in Fig. 2c) features the first five reflections of the austenitic γ matrix. No superstructure reflections originating from ordered γ′ precipitates are found. Very small amounts ($<<$ 1 vol%) of NbC formed during the solidification process are present in the alloy. As all four Rietveld refinements are almost identical, only one exemplary Rietveld plot is shown. All Rietveld refinements can be found in the SI. In general, the diffraction patterns of the respective samples exhibit no visible difference. Solely a small shift of the reflections to lower 2θ angles for the hydrogen-treated specimens can be observed. Fig. 2d) shows increasing lattice parameters for the hydrogen-treated specimens. Considering Bragg's law, $(n\lambda = 2d\sin\theta)$ with the incoming X-ray wavelength (λ), a shift to lower scattering angles (2θ) corresponds to larger lattice plane spacings (d). This aligns well with the expected incorporation of hydrogen within interstitial sites of the austenitic fcc lattice. After approximately 36 h, saturation is observed without further lattice parameter increase, which could be due to a hydrogen saturation in the surface region and the low diffusion rate at room temperature. No further hydrogen uptake may occur with this charging method and the chosen parameters.

It is known that RT electrochemical charging with hydrogen only affects the surface region, as shown e.g. by evaluation of fracture surfaces [44]. This also applies to our cylindrical samples with a diameter of 5 mm. The diffusion coefficient of hydrogen in solution annealed Alloy 718, which was determined via permeation tests at 50 °C, is in the range of 5.3–6.8 $\times$ 10^{-11} cm^2/s [45]. Using this as an approximation for the VDM® Alloy 780 and considering the electrochemical charging times, an average hydrogen diffusion length (L) can be calculated according to Fick's law, i.e. $L = 2\sqrt{Dt}$ with the diffusion coefficient (D) and the charging time (s) [46]. This leads to a calculated average diffusion length of approximately 250 μm for a loading time of 72 h. As the XRD experiments were conducted in Debye-Scherrer geometry, the obtained lattice parameter information contains mainly bulk information that is not affected by hydrogen. As a rough estimation only 2 $\times$ 250 μm out of 5000 μm, i.e., 10 %, is the region where hydrogen is expected from the charging process. The actual value should be even lower, as the diffusion

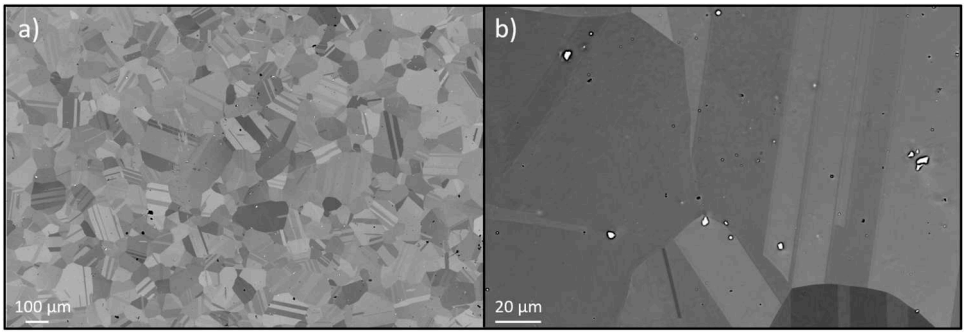

Fig. 1. a) Overview SEM image and b) close-up image of VDM® Alloy 780 in the solutionized and quenched WB0 condition.

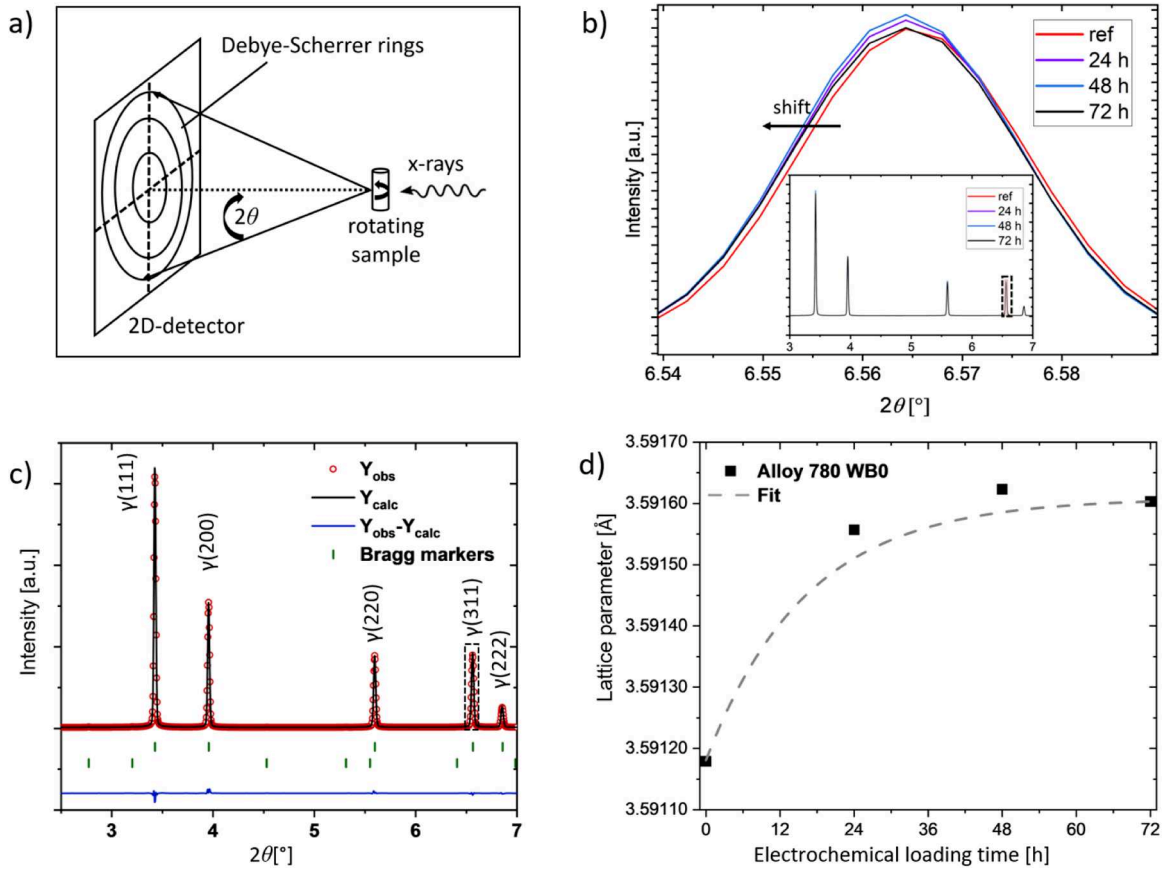

Fig. 2. a) Scheme of the diffraction setup at the P07 beamline. b) γ(311) Bragg reflection to visualize the 2θ shift due to hydrogen charging of VDM® Alloy 780 for different durations. The inset shows the whole diffraction pattern with the dashed line highlighting the γ(311) reflection c) Rietveld refinement of the VDM® Alloy 780 reference specimen. The observed data are shown by red circles, the calculated data by a black line, and the Bragg reflections by the green vertical bars. d) Cell parameters for different hydrogen charging times at RT are shown by the black rectangles and the dotted gray line is a fit of the lattice parameter evolution.

coefficients were determined at 50 °C and the electrochemical loading in this study was carried out at RT. The synchrotron measurements provide an averaged lattice parameter over the illuminated volume. It can therefore be assumed that the lattice parameter in the surface areas is significantly larger than the averaged values from the refinement, but the major bulk part exhibits the reference lattice parameters. In Table 2 the average lattice parameters, the average lattice parameter difference, and the average lattice strain obtained from the Rietveld refinements are given. Additionally, hydrogen is quantified by HGE measurements at 1000 °C and given in wt. and at. ppm, the latter for better comparison of the ratio of metal to hydrogen atoms. The hydrogen concentrations increase with the cathodic charging time. However, a low hydrogen concentration of 0.4 wt. ppm was also found in the reference sample, which is attributed to the manufacturing process of the material, i.e. environmental hydrogen (Table 2).

Table 2
Average RT lattice parameters with different electrochemical charging durations, obtained by individual Rietveld refinements. The lattice constant difference delta as well as the corresponding lattice strain to the hydrogen-free reference are also listed. Hydrogen concentrations obtained by HGE measurements are also given.

Loading time [h]	Ref/0	24	48	72
Lattice constant [Å]	3.59117(4)	3.59154(4)	3.59161(3)	3.59159(5)
Delta [Å]		0.00037	0.00044	0.00042
Lattice strain [%]		0.010	0.012	0.012
H [wt. ppm]	0.4	1.8	2.0	2.9
Delta [wt. ppm]		1.4	1.6	2.5
H [at. ppm]	23.1	103.9	115.4	167.3

It is known that the absorption of hydrogen is a reversible process. However, it was found experimentally that the hydrogen concentration for Alloy 718 alloys is stable at RT for two months [47] respectively one year [48]. To study the effusion of hydrogen in reasonable timespans controlled heating of the samples to 500 °C was performed.

Fig. 3a) shows the development of the cell parameters of hydrogen-loaded VDM® Alloy 780 specimens in comparison to an untreated specimen at varying temperatures. The heating rate was set to 2 °C/min leading to approximately 4 h for each measurement. The lattice parameters were determined via sequential Rietveld refinements of approximately 800 diffraction patterns in total. To prove the validity of the sequential refinements, five refinements (at 100 °C, 200 °C, 300 °C, 400 °C and 500 °C) were performed individually and yielded the same lattice parameters as those obtained through the sequential approach. Again, the determined differences in the cell parameters are small, having a difference of only 4×10^{-4} Å at room temperature, matching the previously determined ex-situ values (cf. Fig. 2d). During heating both samples display an expansion of the cell parameter which coincides with the thermal expansion due to the increased thermal vibration of the atoms. However, while heating the samples, a gradual approach of the curves, i.e. an equalization of the lattice parameters is observed. In Fig. 3b) the mean difference in the lattice parameter is shown for better visualization. The curve shows decreasing values with increasing temperatures, i.e. equalizing lattice parameters and a slight kink at approximately 300 °C, from which the mean difference drops slightly faster. This could be explained by increased diffusion rates of hydrogen at higher temperatures. Both samples reach the same lattice parameters at approx. 500 °C. This indicates the release of interstitial hydrogen and both samples reach the same, hydrogen-free state with equal lattice

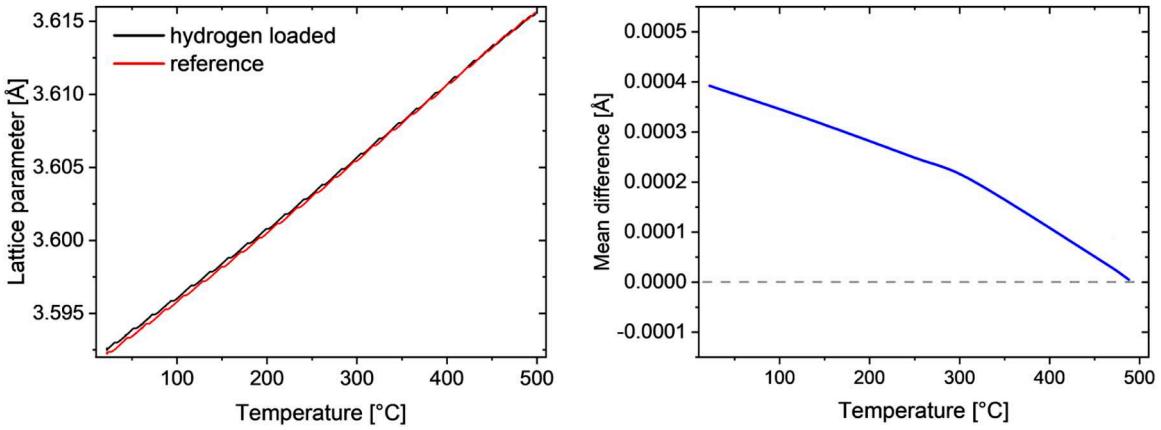

Fig. 3. a) Evolution of the γ phase lattice parameter with temperature for the VDM® Alloy 780 WB0 specimen loaded for 72 h (black) compared to the reference sample (red) and b) the evolution of the mean difference (blue) in lattice constant. The grey dashed line at zero delta is meant to guide the eye.

parameters. To study the temperature-dependent release of hydrogen HGE measurements were performed. Therefore, identical specimens electrochemically loaded for 72 h were used and compared to untreated analogs. The sample preparation for the experiment was carried out with the same charging parameters as the HGE measurements in Table 1.

The reference specimens showed hydrogen values of 0.0 wt. ppm up to the tested temperatures of 400 °C. This shows that temperatures up to 400 °C do not provide enough energy for the effusion of the hydrogen. From 500 °C to 900 °C the measured hydrogen increases to 2.5 wt. ppm. At 1000 °C the value is significantly reduced to 1.9 wt. ppm which is surprising at first glance. The reference measurement at 1000 °C from Table 1 showed only 0.4 wt. ppm, which is significantly lower than the 1.9 wt. ppm of Table 3. This means that the hydrogen uptake, which probably originates from manufacturing or heat treatment processes may vary but is still at a very low level. However, further investigations are required to identify the origin of hydrogen in as-received samples. It therefore makes more sense to compare the delta value here, as it describes the additional hydrogen introduced. At 1000 °C the delta value of the HGE measurements is slightly higher as displayed in Table 3. One possible reason for this is the longer storage time after loading of the diffraction sample. Part of the hydrogen can diffuse out during this period. This highlights how important the reference measurements are for determining the hydrogen content introduced by the loading. For ease of reading, the values from Fig. 4 are shown in the following table.

At 100 °C no hydrogen could be detected for the loaded specimens while with increasing temperatures in steps of 100 °C a linear increase in the hydrogen concentration up to 300 °C was detected. At higher temperatures, the released hydrogen concentrations increase faster. The kink above 300 °C corresponds very well with the diffraction data where the delta value drops faster at temperatures above 300 °C (cf. Fig. 3). In the temperature range between 300 °C and 900 °C, hydrogen concentrations increase almost linearly with a maximum concentration of 5.5 wt. ppm. Interestingly the concentration at 1000 °C is almost 0.5 wt. ppm lower compared to the value at 900 °C, similarly observed in the reference measurement. An explanation for this could be that at 1000 °C changes in the microstructure, like recrystallization, recovery, grain growth, or the dissolution/precipitation of phases occur that hinder the diffusion of hydrogen out of the sample. The alteration observed between 900 °C and 1000 °C corresponds to the γ' solvus temperature

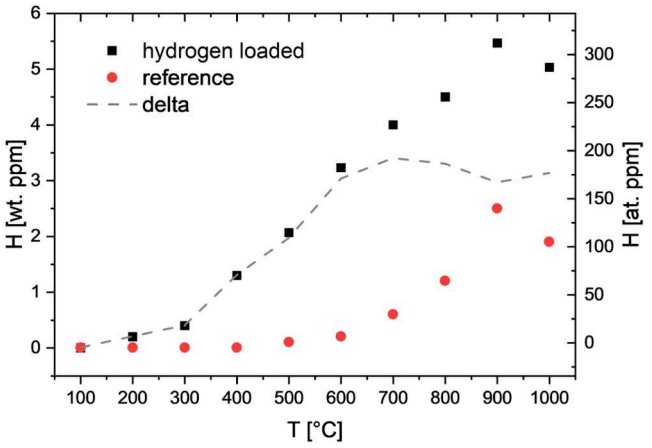

Fig. 4. HGE measurements of VDM® Alloy 780 specimens for the quantification of hydrogen at different temperatures. The black rectangles represent the specimens loaded with hydrogen, the red dots are the reference specimens, and the dashed line is the delta.

being around 990 °C [20,49], which may induce hydrogen diffusion. At 1000 °C recrystallization and recovery may occur, both reducing the dislocation density within the alloy [50]. Since dislocations serve as diffusion paths for hydrogen [51,52], the amount of hydrogen effusing from the specimens might be lowered. Additionally, slight coarsening of the γ matrix grains may occur, leading to larger γ grains and thereby reducing the overall grain boundary surface area. Grain boundaries are also known as diffusion paths for hydrogen [53], which may also explain the lower hydrogen concentrations observed at 1000 °C. Grain growth, recrystallization, recovery or precipitation may also occur at temperatures below 900 °C, however, no alteration in the hydrogen diffusion has been observed. However, further tests need to be carried out to investigate and explain this peculiarity in more detail. Increasing hydrogen values with temperature are due to faster diffusion of hydrogen at elevated temperatures or strongly bound hydrogen that requires high temperatures to overcome its binding energy. Defects or grain boundaries in particular are known to be strong trapping sites [54]. These

Table 3
Temperature-dependent hydrogen quantification by HGE measurements of hydrogen treated and reference specimens.

Temperature [°C]	100	200	300	400	500	600	700	800	900	1000
Loaded H [wt. ppm]	0	0.2	0.4	1.3	2.1	3.2	4.0	4.5	5.5	5.0
Ref [wt. ppm]	0	0	0	0	0.1	0.2	0.6	1.2	2.5	1.9
Delta [wt. ppm]	0	0.2	0.4	1.3	2.0	3.0	3.4	3.3	3.0	3.1

measurements complement the diffraction data and confirm that hydrogen leaves the alloy thermally induced. At temperatures up to 500 °C, the delta values shown in Fig. 4 align with those of the hydrogen-loaded specimens, as the reference specimen exhibits negligible hydrogen amounts. From 600 °C to 1000 °C, the delta remains almost constant, attributed to the increasing hydrogen concentrations effusing from the reference specimens. An explanation for this could be that at temperatures of 500 °C or higher, strongly trapped hydrogen from the manufacturing process is released which is present in the hydrogen treated and the reference specimen in equal amounts. In the diffraction measurements, only the weakly bound interstitial hydrogen dissolved within the fcc lattice is traceable due to its widening of the interatomic distances. This interstitial hydrogen to a large extent effuses out of the sample at temperatures of 500 °C explaining the equalized lattice parameters at 500 °C. It should be noted, however, that the HGE measurements are not fully comparable with the XRD measurements, since the XRD measurements were performed at a constant heating rate, while the HGE measurements were performed at discrete temperatures. Therefore, the specimen measured via diffraction is exposed to elevated temperatures for much longer, i.e. there is more time for the diffusion of hydrogen from the sample. This kinetic effect may explain why the HGE measurements show increasing delta values up to 600 °C. Nevertheless, both measurements support the assumption that interstitially bound hydrogen leaves the crystal lattice by thermally accelerated diffusion.

Finally, tensile tests at RT were also carried out with an identically loaded specimen compared to a hydrogen-free reference.

The mechanical behavior of both samples is similar; however, the flow stress is slightly higher for the reference. Reduced flow stress due to the presence of hydrogen was also observed by Asadipoor et al. in an X70 pipeline steel [55]. A possible explanation for the easier plastic deformation is the decrease in the activation energy for nucleation of dislocations by hydrogen [56]. In the plastic region, the hydrogen-treated specimen and the reference specimen show pronounced work hardening due to the formation and interaction of dislocations. The ultimate tensile strength is higher for the hydrogen-free reference, which is also in accordance with the literature where reduced ultimate tensile strength was observed for steels and Ni-based superalloys [55,57,58]. Elongation at fracture values of approximately 50 % and 44 % of the reference and hydrogen treated, respectively show also the influence of hydrogen. However, the material still exhibits a very

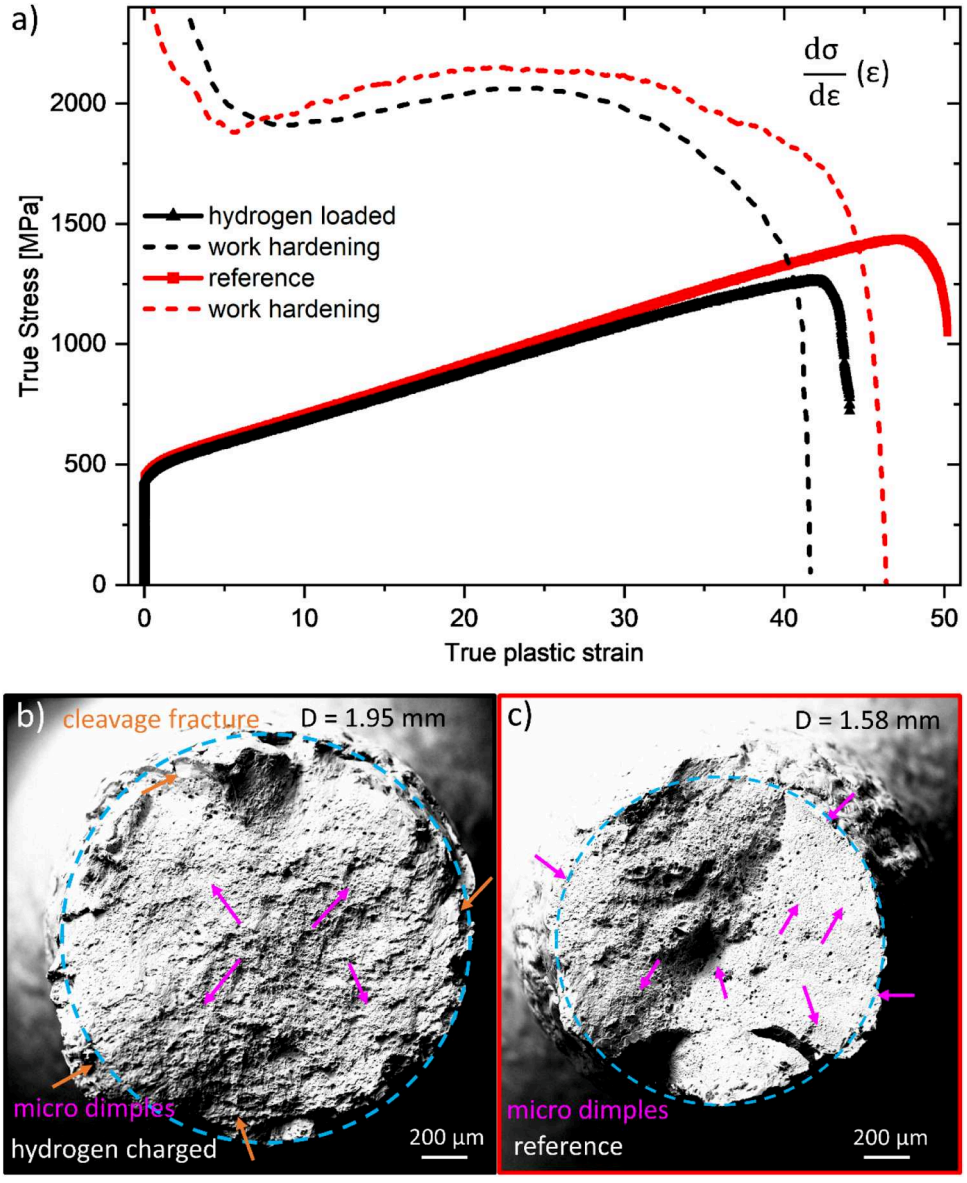

Fig. 5. a) True stress-strain response (solid) of VDM® Alloy 780 at RT and work hardening rate (dashed). b) and c) SEM images of the fracture surfaces. The purple arrows show micro dimples, the orange arrows indicate cleavage fracture, and the blue dashed circle approximates the diameter.

ductile behavior when treated with hydrogen. For age-hardened polycrystalline Ni-based superalloys and advanced high-strength steels incorporated hydrogen typically lead to dramatically reduced elongation at fracture values [59,60]. As the tested VDM® Alloy 780 specimens are solution annealed, i.e. without hardening phase precipitates, the susceptibility to HE is reduced. The work hardening rate is also depicted, showing a similar evolution, i.e. strong decreasing values at the beginning of plastic deformation followed by slightly increasing values to approximately 25 % true plastic deformation. The intersection of the curves where $d\sigma/d\varepsilon = \sigma_{true}$ known as the Considere criterion indicates the onset of unstable deformation, commonly referred to as necking [61]. For the reference specimen, necking initiates at a true plastic strain of 45 %, whereas for the hydrogen-treated specimen, it begins at 41. The interval between the onset of necking and fracture was 4.8 and 2.8 for the reference and hydrogen-treated specimens respectively. This may explain why the diameter of the fracture surface for the reference sample is significantly reduced as compared to the hydrogen-loaded specimen, as can be seen in Fig. 5b) and c).

Additionally, a post-mortem analysis was conducted. The fracture surfaces shown in Fig. 5b) and c) show micro dimples as the predominant failure pattern for the hydrogen-treated and reference specimens. This is as expected for ductile Ni-based alloys after deformation until failure [35]. For the reference specimen, this fracture mode was observed over the entire fracture surface including areas close to the cylinder surface. The hydrogen-treated specimen shows a smoother cleavage-like fracture in the vicinity of the cylinder surface. This confirms the assumption that only the area close to the surface absorbs hydrogen and thus experiences changes in properties during deformation. The transition from brittle to ductile behavior, from the rim to the center of specimens, after electrochemical charging with hydrogen has also been reported for steels and superalloys in literature [4,62]. The necking was measured as a further indicator of HE and is given as a percentage of the initial cross-section. The area of the fracture cross section was determined using the diameter of the blue dashed line in Fig. 5b) and c). From an initial cross-sectional area of approx. 5 mm^2, the cross-section decreased to approx. 2.99 mm^2 for the loaded sample and to approx. 1.96 mm^2 for the unloaded sample, corresponding to 59.9 % and 39.2 % of the cross-section before deformation, respectively. This observation is corroborated by the progression of the true stress-strain curves and the evolution of work hardening. Necking is an indicator of the plasticity of a material; with increasing ductility, necking becomes pronounced. Reduced necking due to the presence of hydrogen was also observed for high-strength steel X80 [63,64]. Post-mortem fractography characterization has confirmed that only the area near the surface is visibly influenced by hydrogen and that quantification of necking is a suitable means of measuring the influence of hydrogen, especially in alloys with high elongation at fracture values.

4. Conclusions

Herein we have presented the influence of hydrogen on the Ni-base superalloy VDM® Alloy 780 in the solution annealed, single-phase fcc state at the atomic level. X-ray diffraction revealed an expansion of the lattice parameter due to the absorption of hydrogen. The observed lattice expansion upon electrochemical hydrogen loading coincides well with the presence of hydrogen occupying interstitial crystallographic sites. Saturation of the lattice parameters was found to be reached after approximately 36 h of electrochemical charging for this specific experiment and specimen geometry. In-situ heating experiments demonstrate the reversibility of the hydrogen uptake, discernible by the equalizing lattice parameter upon effusion of hydrogen at elevated temperatures. Complementary hydrogen quantification via HGE measurements indicates that hydrogen concentrations increase with prolonged charging time. The HGE measurements at different temperatures between 100 °C and 1000 °C underpin that the diffusion of hydrogen strongly depends on the applied temperature and hydrogen allocated at high energy trapping sites requires temperatures of 600 °C or more to overcome the binding energies. The HGE measurements validate the reversibility of hydrogen uptake for weakly bound hydrogen. The tensile tests show only a small influence of hydrogen on the mechanical properties, with a slightly reduced ductility. Fractographic analysis showed that both the hydrogen-treated and the reference specimen, feature micro dimples; however, the hydrogen-loaded specimen shows a cleavage fracture at the rim and reduced necking, i.e., a larger cross-section of the fracture surface. In conclusion, this study has revealed highly interesting results on the role of hydrogen in an austenitic γ phase of a Ni-base superalloy. One of the most important findings is that interstitially dissolved hydrogen completely effuses from the γ phase at 500 °C. At temperatures above 500 °C, further hydrogen effuses but originates from trapping sites with higher binding energies, where it does not affect the lattice parameters of the γ phase. However, future research is necessary to study the impact of hydrogen on a fully age-hardened state of the VDM® Alloy 780 that consists of the more complex γ/γ' microstructure used in high-temperature applications.

CRediT authorship contribution statement

Andreas Stark: Investigation. **Oliver Nagel:** Writing – review & editing, Investigation, Formal analysis. **Alexander Mutschke:** Writing – review & editing, Investigation, Formal analysis. **Massimo Fritton:** Writing – original draft, Investigation, Formal analysis, Conceptualization. **Bodo Gehrmann:** Resources, Investigation. **Masood Hafez-Haghighat:** Writing – review & editing, Resources, Investigation. **Steffen Neumeier:** Writing – review & editing, Supervision, Funding acquisition, Conceptualization. **Ralph Gilles:** Writing – review & editing, Supervision, Project administration, Funding acquisition.

Declaration of Competing Interest

The authors declare that they have no known competing financial interests or personal relationships that could have appeared to influence the work reported in this paper.

Acknowledgments

We gratefully acknowledge DESY (Hamburg, Germany), a member of the Helmholtz Association HGF, for providing the experimental facilities. This research was partially conducted at PETRA III, and we extend our thanks to Norbert Schell and Andreas Stark for their assistance with the HEMS beamline. We also appreciate the financial support from the BMBF Project "An apparatus to study the influence of hydrogen charging and discharging on industrial developed and applied alloys – H2Mat (05K22WO3) and BMBF (05K22WE1).

Declaration of Competing Interest

The authors state that they have no financial interests or personal relationships that could have influenced the work presented in this paper.

Appendix A. Supporting information

Supplementary data associated with this article can be found in the online version at doi:10.1016/j.jallcom.2025.178693.

Data availability

Data will be made available on request.

References

[1] P.C. Okonkwo, E.M. Barhoumi, I. Ben Belgacem, I.B. Mansir, M. Aliyu, W. Emori, P. C. Uzoma, W.H. Beitelmal, E. Akyüz, A.B. Radwan, R.A. Shakoor, A focused review of the hydrogen storage tank embrittlement mechanism process, Int. J. Hydrog. Energy 48 (35) (2023) 12935–12948.

[2] P.V. Petroyiannis, A.T. Kermanidis, P. Papanikos, S.G. Pantelakis, Corrosion-induced hydrogen embrittlement of 2024 and 6013 aluminum alloys, Theor. Appl. Fract. Mech. 41 (1) (2004) 173–183.

[3] M.B. Djukic, G.M. Bakic, V. Sijacki Zeravcic, A. Sedmak, B. Rajicic, The synergistic action and interplay of hydrogen embrittlement mechanisms in steels and iron: localized plasticity and decohesion, Eng. Fract. Mech. 216 (2019) 106528.

[4] S.-I. Lee, J.-M. Lee, S.-Y. Lee, H.-J. Kim, J.-Y. Suh, J.-H. Shim, U.-B. Baek, S.-H. Nahm, J. Lee, B. Hwang, Tensile and fracture behaviors of austenitic high-manganese steels subject to different hydrogen embrittlement test methods, Mater. Sci. Eng. A 766 (2019) 138367.

[5] Y. Du, X. Gao, L. Lan, X. Qi, H. Wu, L. Du, R.D.K. Misra, Hydrogen embrittlement behavior of high strength low carbon medium manganese steel under different heat treatments, Int. J. Hydrog. Energy 44 (60) (2019) 32292–32306.

[6] J. Han, J.-H. Nam, Y.-K. Lee, The mechanism of hydrogen embrittlement in intercritically annealed medium Mn TRIP steel, Acta Mater. 113 (2016) 1–10.

[7] X. Li, J. Zhang, Q. Fu, E. Akiyama, X. Song, Y. Wang, Q. Li, N. Zou, Tensile mechanical properties and fracture behaviors of nickel-based superalloy 718 in the presence of hydrogen, Int. J. Hydrog. Energy 43 (43) (2018) 20118–20132.

[8] R.A. Oriani, P.H. Josephic, Testing of the decohesion theory of hydrogen-induced crack propagation, Scr. Metall. 6 (8) (1972) 681–688.

[9] Z. Tarzimoghadam, D. Ponge, J. Klöwer, D. Raabe, Hydrogen-assisted failure in Ni-based superalloy 718 studied under in situ hydrogen charging: the role of localized deformation in crack propagation, Acta Mater. 128 (2017) 365–374.

[10] C.San Marchi, B.P. Somerday, X. Tang, G.H. Schiroky, Effects of alloy composition and strain hardening on tensile fracture of hydrogen-precharged type 316 stainless steels, Int. J. Hydrog. Energy 33 (2) (2008) 889–904.

[11] R.M. Lindstrom, Prompt-gamma activation analysis, J. Res. Nat. Inst. Stand. Technol. 98 (1) (1993) 127.

[12] S.V. Merzlikin, S. Borodin, D. Vogel, M. Rohwerder, Ultra high vacuum high precision low background setup with temperature control for thermal desorption mass spectroscopy (TDA-MS) of hydrogen in metals, Talanta 136 (2015) 108–113.

[13] Z. Tarzimoghadam, M. Rohwerder, S.V. Merzlikin, A. Bashir, L. Yedra, S. Eswara, D. Ponge, D. Raabe, Multi-scale and spatially resolved hydrogen mapping in a Ni–Nb model alloy reveals the role of the δ phase in hydrogen embrittlement of alloy 718, Acta Mater. 109 (2016) 69–81.

[14] T. Kannengiesser, N. Tiersch, Measurements of diffusible hydrogen contents at elevated temperatures using different hot extraction techniques – an international round robin test, Weld. World 54 (5–6) (2024) R115–R122.

[15] J. Kim, E. Plancher, C.C. Tasan, Hydrogenation-induced lattice expansion and its effects on hydrogen diffusion and damage in Ti–6Al–4V, Acta Mater. 188 (2020) 686–696.

[16] P.E. Irving, C.J. Beevers, Some metallographie and lattice parameter observations on titanium hydride, MT 2 (2) (2024) 613–615.

[17] F. Kümmel, A. Kirchmayer, C. Solís, M. Hofmann, R. Gilles, Deformation mechanisms in Ni-based superalloys at room and elevated temperatures studied by in situ neutron diffraction and electron microscopy, Metals 11 (5) (2021) 719.

[18] C. Solís, J. Munke, M. Bergner, A. Kriele, M.J. Mühlbauer, D.V. Cheptiakov, B. Gehrmann, J. Rösler, R. Gilles, In situ characterization at elevated temperatures of a new Ni-based superalloy VDM-780 premium, Met. Mater. Trans. A 49 (9) (2018) 4373–4381.

[19] C. Solís, J. Munke, M. Hofmann, S. Mühlbauer, M. Bergner, B. Gehrmann, J. Rösler, R. Gilles, In situ characterization at high temperature of VDM Alloy 780 premium to determine solvus temperatures and phase transformations using neutron diffraction and small-angle neutron scattering, Miner. Met. Mater. Ser. (2019) 23–32.

[20] F. Kümmel, M. Fritton, C. Solís, A. Kriele, A. Stark, R. Gilles, Near-surface and bulk dissolution behavior of γ' precipitates in nickel-based VDM® alloy 780 studied with in-situ lab-source and synchrotron X-ray diffraction, Metals 12 (7) (2022) 1067.

[21] C. Solís, J. Munke, M. Bergner, A. Kriele, M.J. Mühlbauer, D.V. Cheptiakov, B. Gehrmann, J. Rösler, R. Gilles, In situ characterization at elevated temperatures of a new Ni-based superalloy VDM-780 premium, Metall. Mater. Trans. A: Phys. Metall. Mater. Sci. 49 (9) (2018) 4373–4381.

[22] C. Solís, J. Munke, M. Hofmann, S. Mühlbauer, M. Bergner, B. Gehrmann, J. Rösler, R. Gilles, In situ characterization at high temperature of VDM Alloy 780 premium to determine solvus temperatures and phase transformations using neutron diffraction and small-angle neutron scattering, Miner. Met. Mater. Ser. (2019) 23–32.

[23] F. Kümmel, A. Kirchmayer, C. Solís, M. Hofmann, S. Neumeier, R. Gilles, Deformation mechanisms in Ni-based superalloys at room and elevated temperatures studied by in situ neutron diffraction and electron microscopy, Metals 11 (5) (2021) 719.

[24] M. Fritton, F. Kümmel, A. Kirchmayer, A. Stark, M. Hafez Haghighat, B. Gehrmann, S. Neumeier, R. Gilles, Investigation of the hot deformation behavior in VDM® alloy 780 by in situ high-energy X-ray diffraction, Metall. Mater. Trans. A (2023).

[25] J. Rösler, T. Hentrich, B. Gehrmann, On the development concept for a new 718-type superalloy with improved temperature capability, Metals 9 (10) (2019) 1130.

[26] J. Botinha, H. Alves, C. Solís, A. Feoktystov, B. Gehrmann, R. Gilles, J. Munke, V. Baran, Study of phase distribution on alloy UNS N07718 in different hardening conditions and its relationship with hydrogen embrittlement susceptibility, in: Proceedings of the NACE - International Corrosion Conference Series, 2019.

[27] L. Liu, K. Tanaka, A. Hirose, K.F. Kobayashi, Effects of precipitation phases on the hydrogen embrittlement sensitivity of Inconel 718, Sci. Technol. Adv. Mater. 3 (4) (2002) 335–344.

[28] Z. Zhang, G. Obasi, R. Morana, M. Preuss, Hydrogen assisted crack initiation and propagation in a nickel-based superalloy, Acta Mater. 113 (2016) 272–283.

[29] L. Liu, C. Zhai, C. Lu, W. Ding, A. Hirose, K.F. Kobayashi, Study of the effect of δ phase on hydrogen embrittlement of Inconel 718 by notch tensile tests, Corros. Sci. 47 (2) (2005) 355–367.

[30] C. Ghica, C. Solís, J. Munke, A. Stark, B. Gehrmann, M. Bergner, J. Rösler, R. Gilles, HRTEM analysis of the high-temperature phases of the newly developed high-temperature Ni-base superalloy VDM 780 Premium, J. Alloy. Compd. 814 (2020) 152–157.

[31] M.C. Rezende, L.S. Araújo, S.B. Gabriel, D.S. Santos, L.H. Almeida, Hydrogen embrittlement in nickel-based superalloy 718: relationship between $\gamma' + \gamma''$ precipitation and the fracture mode, Int. J. Hydrog. Energy 40 (47) (2015) 17075–17083.

[32] Z. Tarzimoghadam, D. Ponge, J. Klöwer, D. Raabe, Hydrogen-assisted failure in Ni-based superalloy 718 studied under in situ hydrogen charging: the role of localized deformation in crack propagation, Acta Mater. 128 (2017) 365–374.

[33] J. Klöwer, O. Gosheva, H.S. Klapper, Z. Tarzimoghadam, Effect of Microstructural Particularities on the Corrosion Resistance of Nickel Alloy UNS N07718 – What Really Makes the Difference?, OnePetro, 2017.

[34] Z. Zhang, K.L. Moore, G. McMahon, R. Morana, M. Preuss, On the role of precipitates in hydrogen trapping and hydrogen embrittlement of a nickel-based superalloy, Corros. Sci. 146 (2019) 58–69.

[35] P.D. Hicks, C.J. Altstetter, Internal hydrogen effects on tensile properties of iron- and nickel-base superalloys, Metall. Trans. A 21 (1) (1990) 365–372.

[36] L. Fournier, D. Delafosse, T. Magnin, Cathodic hydrogen embrittlement in alloy 718, Mater. Sci. Eng. A 269 (1) (1999) 111–119.

[37] M. Hoelzel, S.A. Danilkin, H. Ehrenberg, D.M. Toebbens, T.J. Udovic, H. Fuess, H. Wipf, Effects of high-pressure hydrogen charging on the structure of austenitic stainless steels, Mater. Sci. Eng. A 384 (1) (2004) 255–261.

[38] M. Fritton, F. Kümmel, A. Kirchmayer, A. Stark, M. Hafez Haghighat, B. Gehrmann, S. Neumeier, R. Gilles, Investigation of the hot deformation behavior in VDM® alloy 780 by in situ high-energy X-ray diffraction, Metall. Mater. Trans. A (2023) 1–15.

[39] N. Schell, A. King, F. Beckmann, T. Fischer, M. Müller, A. Schreyer, The high energy materials science beamline (HEMS) at PETRA III, Mater. Sci. Forum 772 (2014) 57–61.

[40] A.P. Hammersley, FIT2D: a multi-purpose data reduction, analysis and visualization program, J. Appl. Crystallogr. 49 (2) (2016) 646–652.

[41] J. Rodríguez-Carvajal, Recent advances in magnetic structure determination by neutron powder diffraction, Physica B 192 (1) (1993) 55–69.

[42] W.A. Dollase, Correction of intensities for preferred orientation in powder diffractometry: application of the March model, J. Appl. Crystallogr. 19 (4) (1986) 267–272.

[43] C. Solís, A. Kirchmayer, I. da Silva, F. Kümmel, S. Mühlbauer, P. Beran, B. Gehrmann, M.H. Haghighat, S. Neumeier, R. Gilles, Monitoring the precipitation of the hardening phase in the new VDM® alloy 780 by in-situ high-temperature small-angle neutron scattering, neutron diffraction and complementary microscopy techniques, J. Alloy. Compd. 928 (2022) 167203.

[44] D. Sampath, R. Akid, R. Morana, Estimation of crack initiation stress and local fracture toughness of Ni-alloys 945X (UNS N09946) and 718 (UNS N07718) under hydrogen environment via fracture surface topography analysis, Eng. Fract. Mech. 191 (2017) 324–343.

[45] J.J.M. Jebaraj, D.J. Morrison, I.I. Suni, Hydrogen diffusion coefficients through Inconel 718 in different metallurgical conditions, Corros. Sci. 80 (2014) 517–522.

[46] X. Li, J. Zhang, Q. Fu, X. Song, S. Shen, Q. Li, A comparative study of hydrogen embrittlement of 20SiMn2CrNiMo, PSB1080 and PH13-8Mo high strength steels, Mater. Sci. Eng. A 724 (2018) 518–528.

[47] N. Ehrlin, C. Bjerkén, M. Fisk, Cathodic hydrogen charging of Inconel 718, AIMS Mater. Sci. 3 (4) (2016) 1350–1364.

[48] H.R. Gray, Embrittlement of nickel-, cobalt-, and iron-base superalloys by exposure to hydrogen, 1975.

[49] J. Sharma, M.H. Haghighat, B. Gehrmann, C. Moussa, N. Bozzolo, Dynamic and post-dynamic recrystallization during supersolvus forging of the new nickel-based superalloy—VDM alloy 780, Superalloys 2020, Springer International Publishing, Cham, Switzerland, 2020, pp. 450–60.

[50] N. Holtham, N. Brooks, L. Hackel, K. Davami, Investigation of high-temperature recovery and recrystallization behavior in a single crystal Ni-based superalloy treated with shot peening and laser peening, Met. Mater. Int. (2024) 1–12.

[51] A.M. Brass, A. Chanfreau, Accelerated diffusion of hydrogen along grain boundaries in nickel, Acta Mater. 44 (9) (1996) 3823–3831.

[52] J. Chêne, A.M. Brass, Hydrogen transport by mobile dislocations in nickel base superalloy single crystals, Scr. Mater. 40 (5) (1999) 537–542.

[53] S. Lynch, Hydrogen embrittlement phenomena and mechanisms, Corros. Rev. 30 (3–4) (2012) 105–123.

[54] A. Raina, V.S. Deshpande, N.A. Fleck, Analysis of thermal desorption of hydrogen in metallic alloys, Acta Mater. 144 (2018) 777–785.

[55] M. Asadipoor, A. Pourkamali Anaraki, J. Kadkhodapour, S.M.H. Sharifi, A. Barnoush, Macro- and microscale investigations of hydrogen embrittlement in X70 pipeline steel by in-situ and ex-situ hydrogen charging tensile tests and in-situ electrochemical micro-cantilever bending test, Mater. Sci. Eng. A 772 (2020) 138762.

[56] A. Barnoush, N. Kheradmand, T. Hajilou, Correlation between the hydrogen chemical potential and pop-in load during in situ electrochemical nanoindentation, Scr. Mater. 108 (2015) 76–79.
[57] K.G. Reddy, S. Arumugam, T.S. Lakshmanan, Hydrogen embrittlement of maraging steel, J. Mater. Sci. 27 (19) (1992) 5159–5162.
[58] F. Han, S. He, M. Liu, X.T. Zhou, Hydrogen embrittlement susceptibility of a Ni-16Mo-7Cr base superalloy, Mater. Sci. Eng. A 733 (2018) 291–298.
[59] M. Asadipoor, J. Kadkhodapour, A. Pourkamali Anaraki, S.M.H. Sharifi, A. C. Darabi, A. Barnoush, Experimental and numerical investigation of hydrogen embrittlement effect on microdamage evolution of advanced high-strength dual-phase steel, Met. Mater. Int. 27 (7) (2021) 2276–2291.
[60] T. Depover, D. Pérez Escobar, E. Wallaert, Z. Zermout, K. Verbeken, Effect of hydrogen charging on the mechanical properties of advanced high strength steels, Int. J. Hydrog. Energy 39 (9) (2014) 4647–4656.
[61] C.E. Slone, C.R. LaRosa, C.H. Zenk, E.P. George, M. Ghazisaeidi, M.J. Mills, Deactivating deformation twinning in medium-entropy CrCoNi with small additions of aluminum and titanium, Scr. Mater. 178 (2020) 295–300.
[62] X. Lu, D. Wang, D. Wan, Z.B. Zhang, N. Kheradmand, A. Barnoush, Effect of electrochemical charging on the hydrogen embrittlement susceptibility of alloy 718, Acta Mater. 179 (2019) 36–48.
[63] S.P. Trasatti, E. Sivieri, F. Mazza, Susceptibility of a X80 steel to hydrogen embrittlement, Mater. Corros. 56 (2) (2005) 111–117.
[64] I. Moro, L. Briottet, P. Lemoine, E. Andrieu, C. Blanc, G. Odemer, Hydrogen embrittlement susceptibility of a high strength steel X80, Mater. Sci. Eng. A 527 (27) (2010) 7252–7260.